EGTRIB Journal
JOURNAL OF
THE EGYPTIAN SOCIETY OF TRIBOLOGY
VOLUME 21, No. 2, April 2024, pp. 79 – 92 **ISSN 2090 - 5882**
(Received November 21. 2023, Accepted in final form February 16. 2024) **jest.journals.ekb.eg**

THERMO-MECHANICAL MODEL AND VALIDATION FOR FRICTION STIR WELDING OF SUPER DUPLEX STAINLESS STEEL SAF 2507

Ali A. S.[1], Sakr Kh. M.[2], Elsoeudy R. I.[1] and El-Shazly M. H.[3]

[1]Mechanical Engineering Dept., Faculty of Engineering, Suez Canal University,
[2]Engineer Officer in the Egyptian Armed Forces,
[3] Department of Mechanical Design and Production Engineering, Faculty of Engineering, Cairo University, Giza, EGYPT.

ABSTRACT
This paper presents a comprehensive simulation study of Friction Stir Welding (FSW) applied to super duplex stainless steel SAF2507 (UNS S32750)[1]. Two numerical methods, coupled Euler-Lagrange and smoothed particle hydrodynamics, are employed to model the FSW process, [2, 3]. The simulations include essential welding parameters: welding velocity, rotation velocity, tilt angle, and axial force, [4]. To ensure model accuracy and reliability, the results are rigorously validated against experimental data. Two validation methods are utilized, enhancing the robustness of the simulation outcomes. This research contributes valuable insights into FSW processes for super duplex stainless steel SAF2507, serving as a dependable foundation for further exploration and optimization of welding parameters in manufacturing applications.

KEYWORDS
Friction stir processing, thermo-mechanical FEM, coupled Euler Lagrangian, smoothed particles hydrodynamics, super duplex stainless steel, SAF 2507.

INTRODUCTION
Super-duplex stainless steel (SDSS) stands out as a highly utilized alloy in both marine and petrochemical industries, owing to its remarkable mechanical properties and corrosion resistance. This alloy is distinguished by its dual-phase structure comprising ferrite (α) and austenite (γ). This characteristic phase balance of ferrite and austenite not only enhances the tensile and fatigue strength of SDSS but also imparts commendable toughness, even at lower temperatures. Additionally, SDSS exhibits favorable formability and weld ability, along with robust resistance to pitting and general corrosion.

A key contributor to the exceptional corrosion resistance of SDSS is the Pitting Resistance Equivalence (PRE), surpassing 40%. This heightened PRE is attributed to the presence of essential alloying elements such as nickel (Ni), chromium (Cr), nitrogen (N), and molybdenum (Mo), [5]. The amalgamation of these elements not only fortifies

the corrosion resistance but also augments the overall performance and longevity of super-duplex stainless steel in demanding industrial applications.

Friction stir processing (FSP) stands as a notable advancement in materials enhancement, stemming from the solid-state welding technique, friction stir welding (FSW). The inception of FSW in the 1990s by the welding institute marked a significant milestone, offering a myriad of benefits, including improved mechanical properties and reduced material distortion when compared to traditional fusion welding methods, [6].

Building upon the principles of FSW, FSP introduces a novel approach to material modification. A specially designed rotating tool applies heat through friction onto the alloy, with combined rotational and translational motions along the desired path. This unique process softens the material while effectively stirring it, as depicted in Fig. 1. The resultant enhancement in mechanical properties is achieved by strategically altering the microstructure and eliminating internal voids or defects.

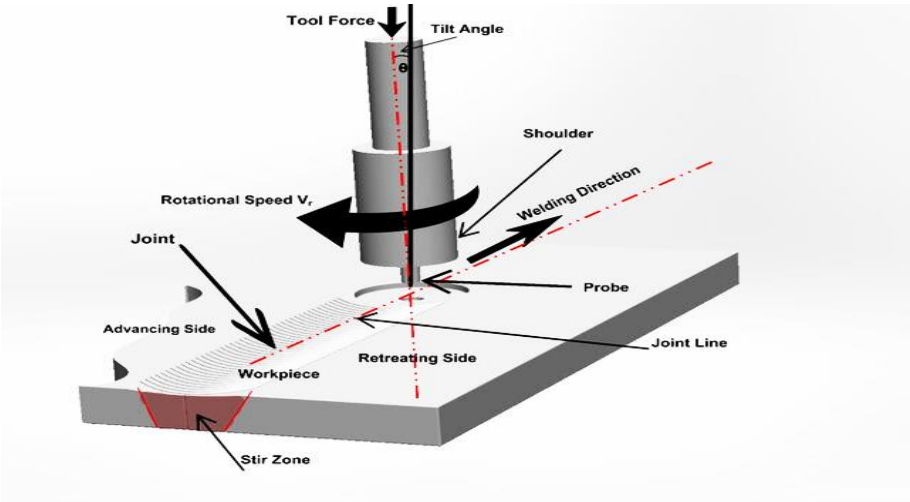

Fig. 1 Schematic diagram of FSP, [7].

To effectively optimize FSP as a technique for material enhancement or grain refinement, it becomes crucial to minimize grain growth. This can be achieved by strategically adjusting parameters such as rotational speed, feed rate, axial force ,and tool tilt angle, [8, 9]. Through meticulous control of these variables, the process can be fine-tuned to yield superior outcomes, emphasizing the importance of precise parameter manipulation in achieving desired material properties and structural characteristics.

Friction Stir Processing (FSP) gives rise to three distinctive metallurgical zones: The Stir Zone (SZ), also known as the Nugget Zone (NZ) when compared to conventional welding processes, the Thermomechanical Affected Zone (TMAZ), and the Heat-Affected Zone (HAZ). The Stir Zone exhibits a recrystallized and fine-grained structure primarily attributed to dynamic recrystallization and straightforward plastic deformation, [10].

In order to enhance our comprehension of the issue and reduce the need for extensive experimental work, it is imperative to employ advanced finite element models. These models should possess the capability to simulate Friction Stir Processing (FSP)

effectively, allowing for the accurate prediction of the ensuing thermal profile, substantial deformation, and assessment of residual stresses under varying rotational and translational speeds.

Two simulation methods, coupled Euler Lagrangian and SPH, have been employed to model FSW in super duplex stainless steel. The coupled Euler Lagrangian method CEL, [11, 12] provides a detailed representation of material behavior and allows for a comprehensive analysis of the thermal and mechanical aspects of the process. On the other hand, the SPH method[13][14], known for its ability to handle large deformations and complex geometries, offers an alternative perspective on FSW simulations.

Material Specification

Super duplex stainless steel SAF 2507 (UNS S32750) alloy is typically characterized by low weld ability when subjected to traditional fusion welding processes. In this research, the plasticity of the material is modeled using the Johnson-Cook model, [15]:

$$\boldsymbol{\sigma = [A + B.(\varepsilon^{-pl})^{n}][1 + C.\ln\left(\frac{\dot{\varepsilon}_{pl}}{\dot{\varepsilon}_{\circ}}\right)][1 - (\frac{T - T_{ref}}{T_{melt} - T_{ref}})^{m}]}$$

with: ε^{-pl} - the effective plastic strain; $\dot{\varepsilon}_{pl}$- is the effective plastic strain rate; $\dot{\varepsilon}_{\circ}$ - is the normalizing strain rate; n, and m are material constants; C represents strain rate sensitivity; T_{ref} is the temperature at which we determine the parameters A, B, n; T solid is the material's solidification temperature, were taken from reference, [16].

Table 1. Constants for Johnson-Cook material model, [16]

Material	T_{melt}	A (MPa)	B (MPa)	C	n	m
SDSS SAF 2507	1400	342	510	0.047	0.5	0.33

The temperature-dependent thermal and mechanical properties were taken into account. The material behavior is characterized by an elastic-perfectly plastic model, incorporating the influence of temperature. As illustrated in Fig. 2, the temperature-dependent properties examined in this research encompass the modulus of elasticity (E), yield strength (s_y), thermal expansion (α), thermal conductivity (k), and specific heat (Cp). Meanwhile, certain physical parameters, including density (7800 kg/m^3) and Poisson's ratio (0.27), are considered constant, independent of temperature.

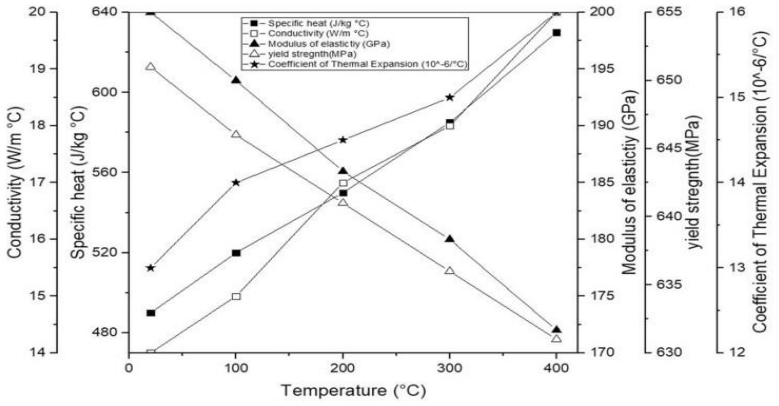

Fig. 2 Temperature-dependent properties of SAF 2507, [17].

Modeling Methods:

- **Coupled Euler Lagragian Method**
- **Part Geometry and Definition**

In our CEL method simulation, critical components have been defined in the part module. The super duplex stainless steel work piece, identified as "Euler" and illustrated in Fig. 3 (a), is characterized by a 3D Eulerian domain with dimensions of 100x200x6 mm. This particular representation is chosen to effectively model the flow-based behavior inherent in Friction Stir Welding (FSW). Furthermore, the simulation incorporates a 3D deformable "reference" part, as depicted in Figure 3 (b), and a 3 D deformable rigid "tool," illustrated in Figure 3 (c), crafted from tungsten carbide. The dynamic behavior of the tool during FSW is aptly captured through the application of the Lagrangian formulation. This specific tool geometry illustrated in Figure 3 (d) and material composition were chosen from, [18].

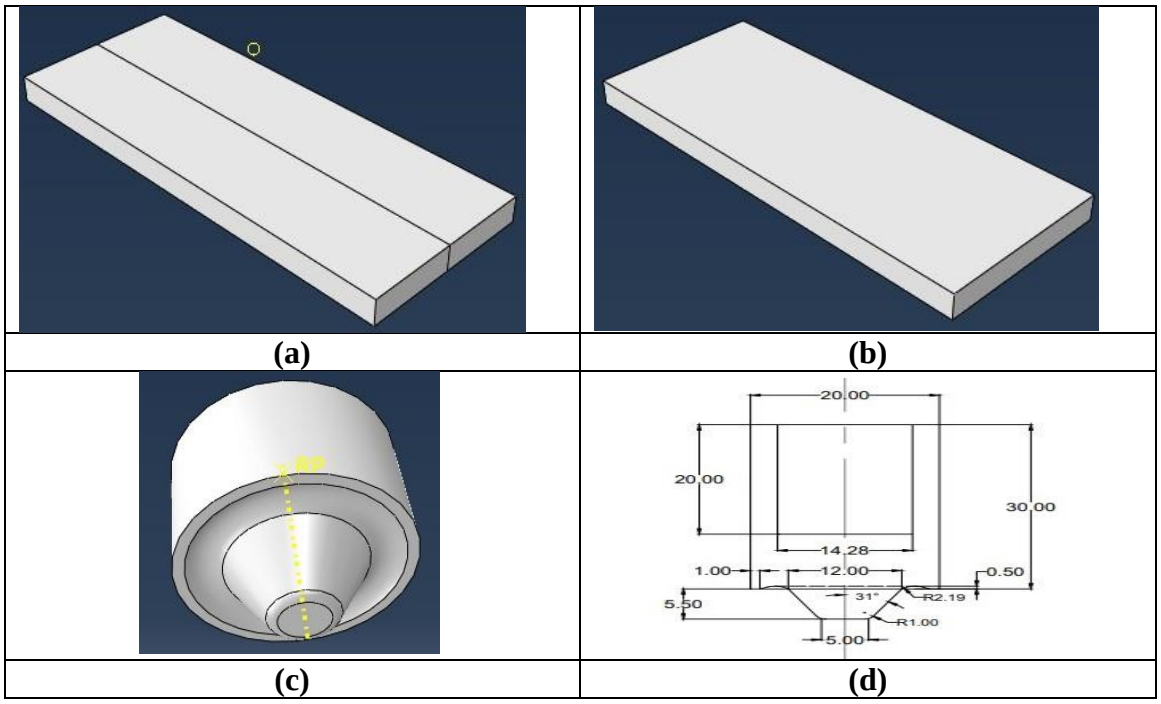

Figure 3. Coupled Eulerian-Lagrangian parts: a) Work piece; b) Reference; c) Tungsten Carbide Tool: d) Tool Geometry, [18].

Interaction module

The interaction manager properties have been carefully defined to model contact behavior during Friction Stir Welding (FSW). For tangential behavior, a penalty-based friction formulation with a friction coefficient of 0.4 has been selected, providing insights into the sliding dynamics at the contact interface. The consideration of heat generation involves default settings for the fraction of dissipated energy caused by friction or electric current that is converted to heat and the fraction of converted heat distributed to the slave surface. The type of the interaction manager chosen is "general contact (explicit)", indicating an explicit treatment of contact interactions.

Load and boundary condition manager

The module load manager is set to apply a pressure load from step 1 to step 3, with a magnitude of 47.7 MPa. This pressure force is calculated based on an axial force of 15 kN applied to the tool, which has a diameter of 20 mm. In Fig. 4, the boundary condition manager for our simulation, three distinct boundary conditions have been meticulously defined to accurately capture the complexities of the Friction Stir Welding (FSW) process. In the initial step, BC1 enforces a fixed boundary condition (Encastre), restraining all translational and rotational degrees of freedom (U1 = U2 = U3 = UR1 = UR2 = UR3 = 0). BC2, implemented during step 1, introduces a rotation and displacement boundary condition to replicate the tool's plunging motion, with a specified displacement of 5.5 mm. In step 1, BC3 modifies the boundary condition to specify an angular velocity of 400 rpm, capturing the tool's rotational dynamics. Furthermore, in step 3, BC3 is adjusted to reflect a welding velocity of 25 mm/min.

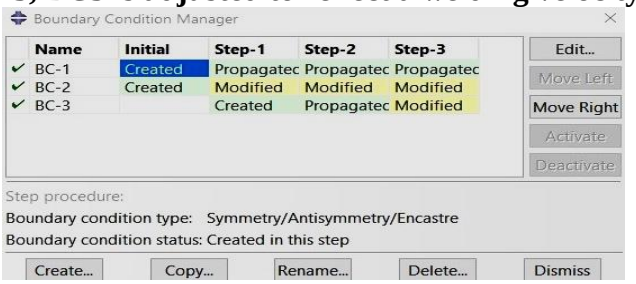

Fig. 4 Boundary condition manager.

Element selection and mesh

In the mesh module, our focus is on the Eulerian representation of the work piece, a total of 3000 elements have been allocated to ensure a fine mesh resolution. The chosen element library is explicit, catering specifically to the Eulerian formulation for thermal coupling.

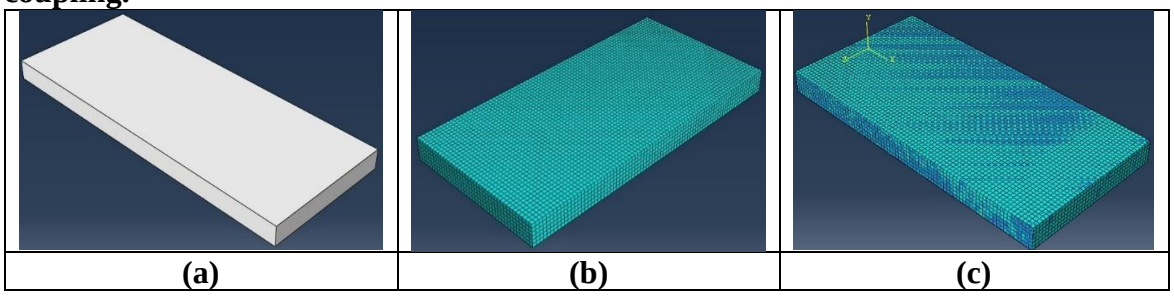

(a) **(b)** **(c)**

Fig. 5 Coupled Eulerian-Lagrangian formulation: a) Lagrangian body; b) Eulerian body; c) coupled Eulerian-Lagrangian.

Problem in Tool Tilt Angle Modification

While using the coupled Eulerian-Lagrangian (CEL) method for FSW simulation, a problem occurs in adjusting boundary conditions for fixing plates, plunging, dwelling and rotating the tool. The problem stemmed because a single reference point in the tool needed modifications for different steps involving various coordinate systems due to the tool's tilt angle with local coordinate system for plunging, dwelling and rotation tool and global coordinate system for welding velocity. This dual-coordinate setup resulted in errors, hindering the tool's interaction with Eulerian plates. To address this, the Smoothed Particle Hydrodynamics (SPH) method used. This switch offers a more

adaptable way to represent material behavior, making the simulation of the intricate FSW process smoother and more accessible.

Smoothed Particle Hydrodynamics (SPH) Method
Part Geometry and Definition
Super duplex stainless steel (SDSS) SAF2507 plates, with dimensions measuring 210 × 100 × 6.5 mm, [17], served as the primary work piece for Friction Stir Welding (FSW) simulations. The welding process was conducted using a specialized tool, 20 mm shoulder polycrystalline cubic boron nitride (PCBN) tool Q70. The tool featured a conical pin with a length of 5.2 mm, radius 5mm with θ equal 30˚, as illustrated in Figure 6. This specific tool geometry and material composition were chosen, [19].

1.1.1 interaction module
In the Interaction module, we established two crucial interactions to ensure realistic contact behavior within the Friction Stir Welding (FSW) simulation. The first interaction, a General Contact, addresses overall contact interactions between different components within the assembly, providing a global perspective. Meanwhile, the second interaction, Surface-to-Surface Contact, offers a more localized and detailed approach, focusing on specific contact conditions between work piece and die.

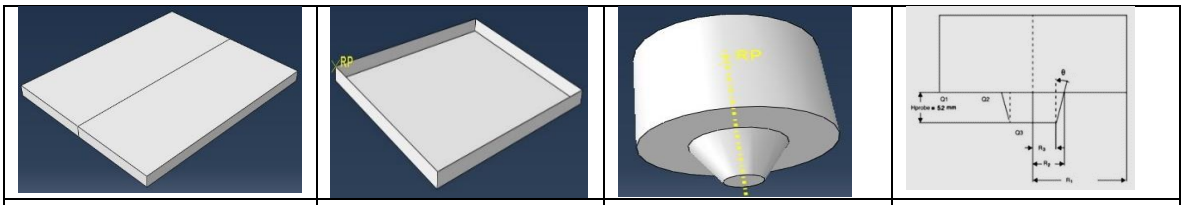

(a)	(b)	(c)	(d)

Fig. 6 SPH parts: a) Work piece; b) Die; c) PCBN tool: d) Tool Geometry, [17].

For the Contact Property Interaction, the tangential behavior to enhance the accuracy of the simulation. The friction formulation is set to penalty, with isotropic directionality, and a friction coefficient of 0.2, [20]. This configuration ensures a realistic representation of the frictional forces at play during the FSW process. Additionally, the settings for Heat Generation include default values for the fraction of dissipated energy converted by friction or electric currents and the distribution of converted heat to the slave surface.

In the Constraint Manager, we introduced two essential rigid body constraints. The first constraint is assigned to the tool, ensuring its rigidity throughout the simulation and restricting unwanted deformations. Similarly, the second constraint is applied to the die, maintaining its rigidity and preventing excessive movement.

Load and boundary condition manager
In Fig. 7 a pressure force of 8.8E+07 Pa, converted from an axial force of 27.7 kN, is applied to the simulation model to represent the forces involved in the FSW process.

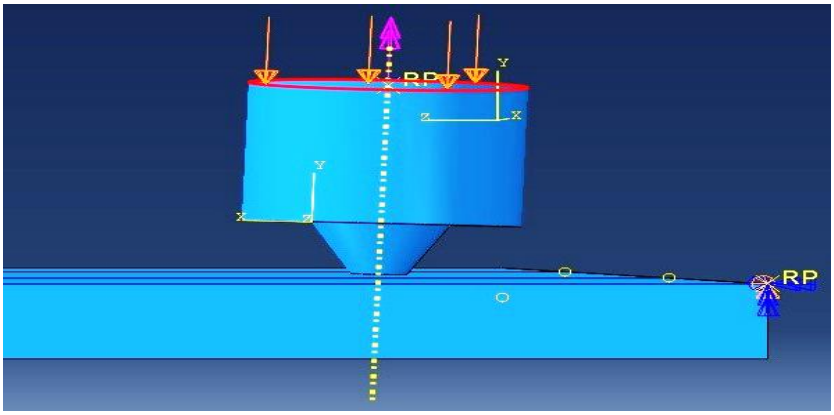

Fig. 7 pressure force Calculated based on axial force.

In Fig. 8, a set of five constraints (BC) has been applied to capture the complexities of the FSW simulation with a newly defined coordinate system. The new coordinate system incorporates a 2-degree tilt of the tool's Y-axis from the global coordinate system.

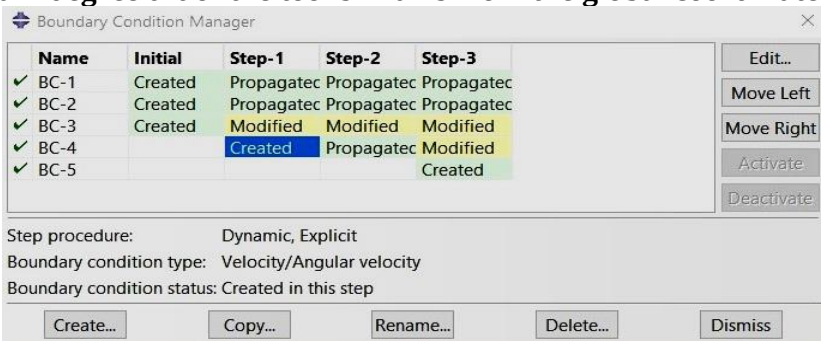

Fig. 8 Boundary condition manager.

Element selection and mesh

In this study, as illustrated in Fig. 9, the mesh comprises 58,800 elements meticulously arranged to ensure accuracy. An explicit element library, specifically emphasizing the 3D stress family is employed. The mesh configuration facilitates seamless conversion to particles.

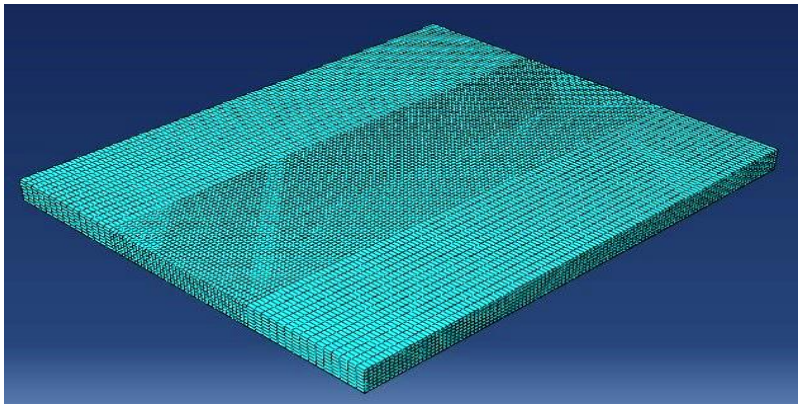

Fig. 9 Meshing of work piece.

RESULTS AND DISCUSSION
Smoothed Particle Hydrodynamics (SPH) Results

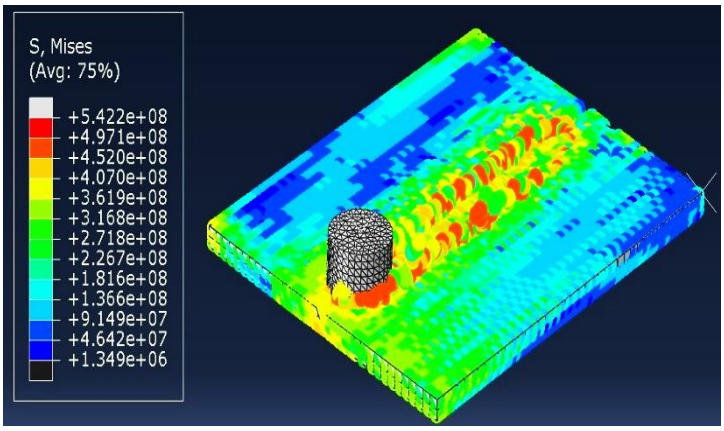

Fig. 10 FSW von-misses stress.

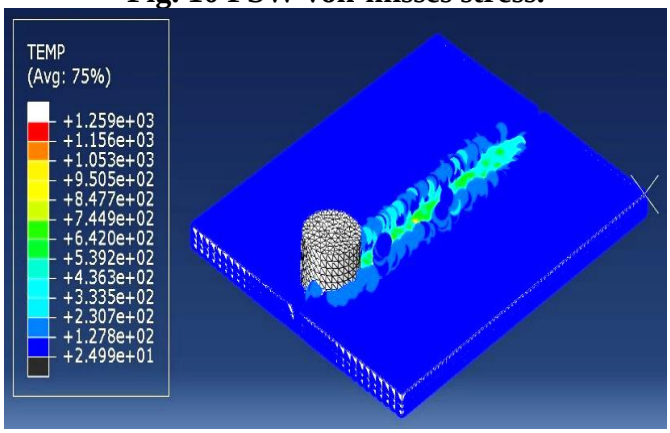

Fig. 11 FSW temperature distribution.

In Figs. 10, 11, the chosen process parameters, including a tool tilt angle of 3 degrees, a welding velocity of 25 mm/min, rotation velocity set at 400 rpm, and an axial load of 15 kN, the maximum temperature attained during the simulation is recorded at 1159 degrees Celsius and the maximum von Mises stress reached 5.422E+08 Pa.

1.2 Coupled Euler Lagragian Results

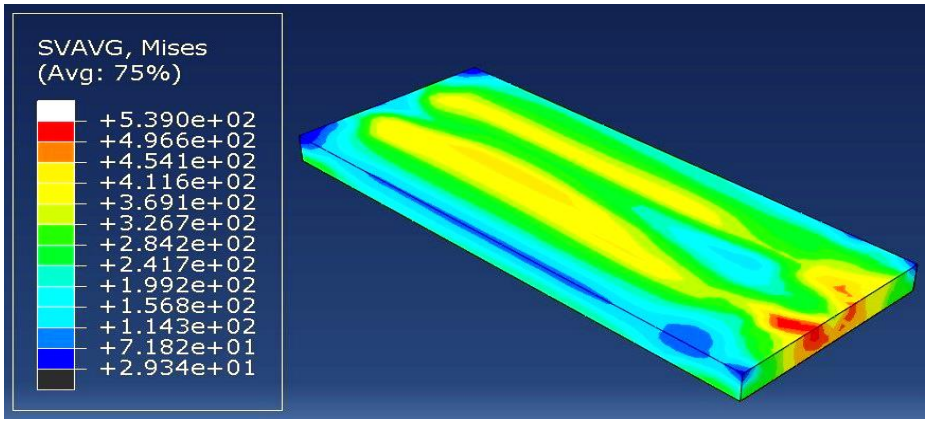

Fig. 12 FSW von-misses stress.

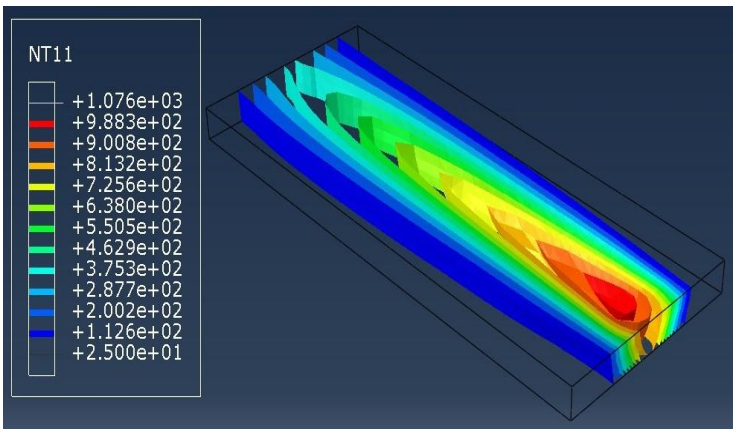

(a)

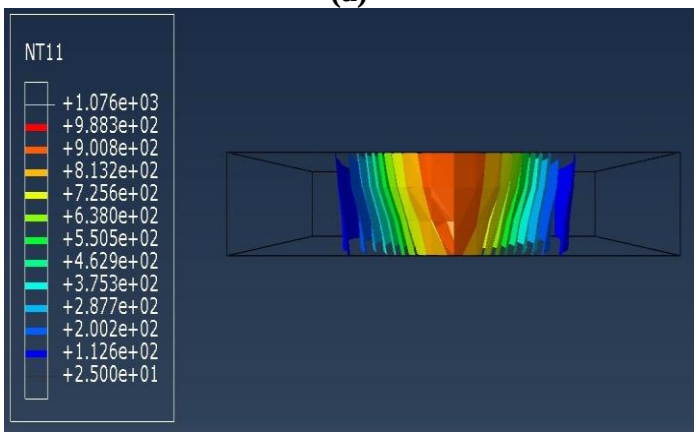

(b)

Fig. 13 FSW temperature distribution, a) Welding direction; b) Work piece thickness.

In Fig. 12, 13, (a, b), the chosen process parameters, including a tool tilt angle of 0 degree, a welding velocity of 25 mm/min, rotation velocity set at 400 rpm, and an axial load of 15 kN, the maximum temperature attained during the simulation is recorded at 1076 degrees Celsius and the maximum von Mises stress reached 5.390 E+02 MPa.

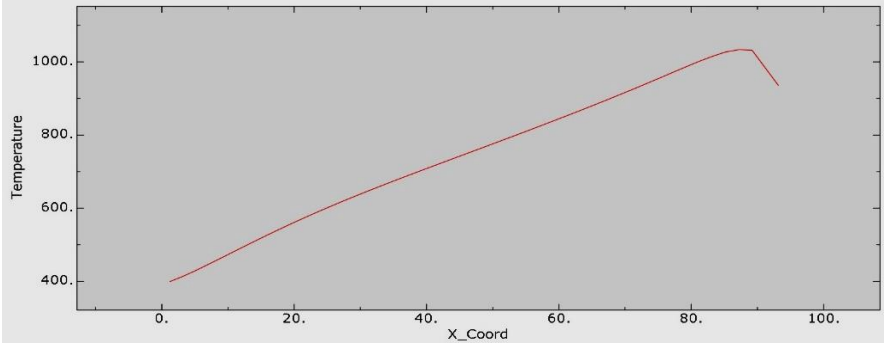

Fig. 14 Temperature distribution along welding direction.

Figure 14 illustrates the temperature variation along the work piece during the welding process. The temperature at the beginning of the work piece is recorded as 400 degrees Celsius, while the maximum temperature at the end of the work piece reaches 1076 degrees Celsius. The chosen process parameters, including a tool tilt angle of 0 degree,

a welding velocity of 25 mm/min, rotation velocity set at 400 rpm, and an axial load of 15 kn.

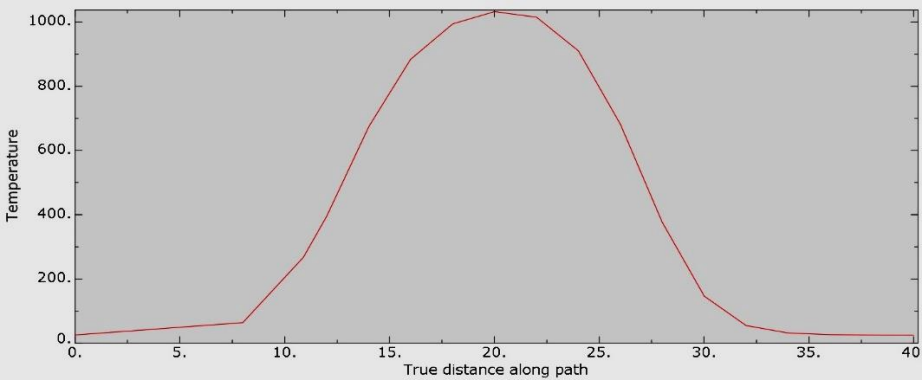

Fig. 15 Temperature distribution along transverse direction.

The temperature distribution along the transverse direction at a distance of 95 mm from the beginning of the FSW process is depicted in Fig. 15. This profile provides insights into how the temperature varies across the work piece width at this specific location during the welding operation. The recorded temperatures contribute to a comprehensive understanding of the thermal behavior and heat distribution in the transverse direction, aiding in the optimization of FSW parameters for enhanced welding outcomes.

Validation with Experimental Results

In order to establish the accuracy and reliability of the finite element models developed in Abaqus for simulating friction stir processing (FSP) in super duplex stainless steel, a rigorous validation process has been conducted. The validation specifically compares our numerical simulations with the experimental results, [17]. The focus of this validation is on key parameters crucial to the FSP process, namely maximum temperature. By aligning our simulation outcomes with the experimental results, Abaqus models accurately capture the thermo-mechanical behavior of super duplex stainless steel during FSP is aimed to ensure. This meticulous comparison provides a comprehensive assessment of the fidelity of our numerical predictions, validating the suitability of our computational approach for predicting and optimizing FSP processes in challenging materials.

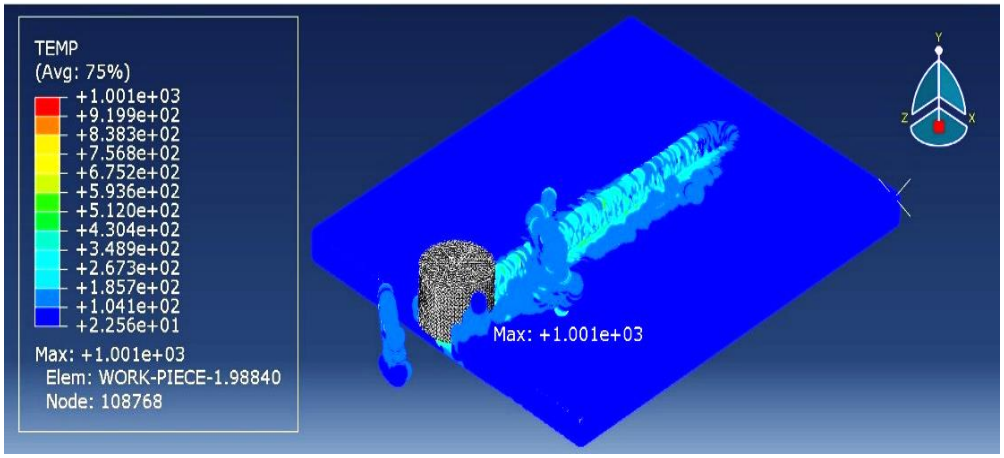

Fig. 16 Maximum temperature from Abaqus Simulation (SPH Method).

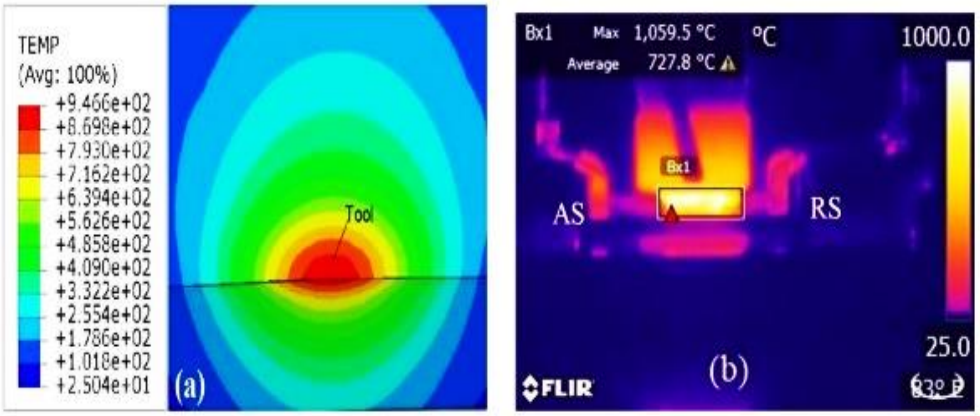

Fig. 17 Temperature distribution during welding,
(a) heat source model and (b) experimental infrared camera, [17].

Smoothed Particle Hydrodynamics (SPH) method for FSW simulation showcases a meticulous comparison between experimental and simulated results. The work piece, composed of SDSS SAF2507 plates with dimensions 210 × 100 × 6.5 mm, is subjected to the PCBN tool Q70 with a shoulder radius of 20 mm, pin radius of 5 mm, and a length of 5.2 mm. The tool's tilt angle 2 degrees is applied. With a rotation velocity of 400 rpm, welding velocity of 100 mm/min, and axial force of 27.7 kn. in figure 16 and 17, the simulation results are in close agreement with experimental data. This validation reinforces the accuracy and reliability of the SPH method in capturing the intricate dynamics of the Friction Stir Welding (FSW) process for SDSS SAF2507, showcasing its potential for robust simulation in real-world applications.

Validation between SPH and CEL numerical methods.

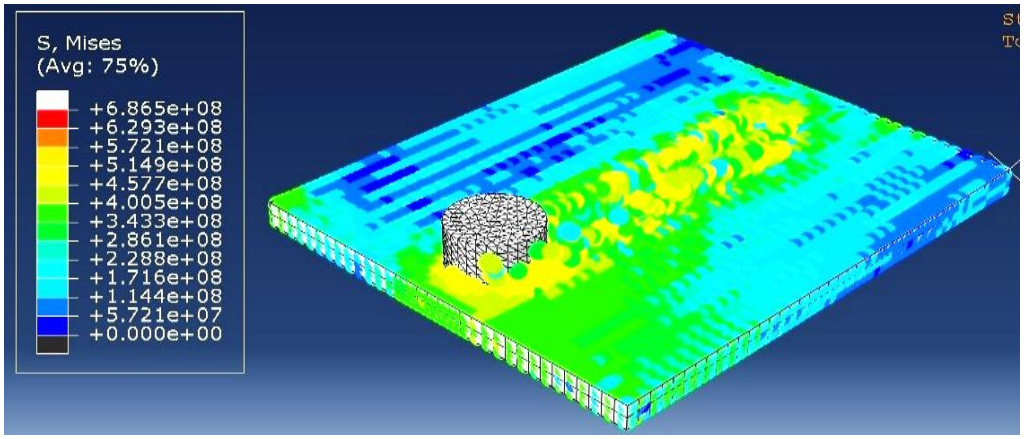

Fig. 18 Von. mises stress (SPH Method).

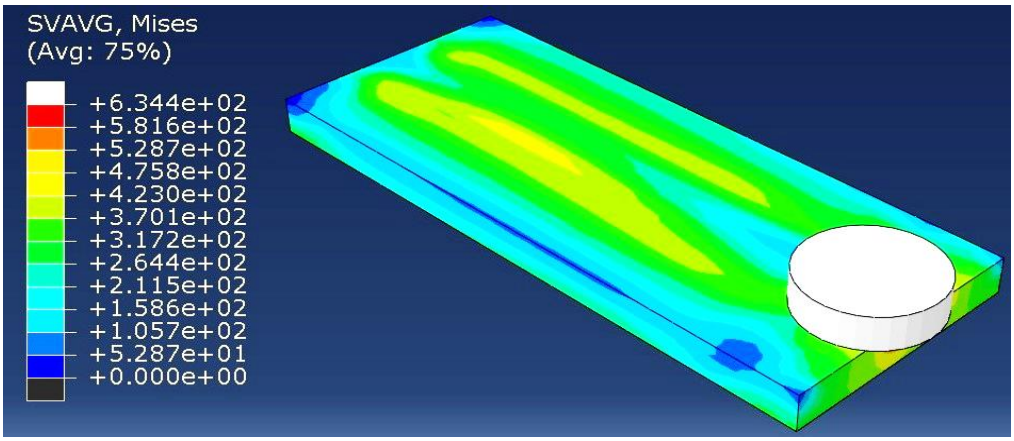

Fig. 19 Von. mises stress (CEL Method).

Figures 18, 19 present a direct comparison between the outcomes achieved through the Coupled Euler Lagrangian (CEL) method and the Smoothed Particle Hydrodynamics (SPH) method. The Von Mises stress is emphasized for specific parameters, including a tilt angle of 0 degrees, rotation velocity of 400 rpm, welding velocity of 25 mm/min, and an axial force of 15 kN. The validation images clearly showcase the concordance and discrepancies in stress values between the two simulation methods. This targeted examination plays a pivotal role in validating the dependability and precision of the simulation models, contributing significantly to the enhancement of FSW simulation techniques for superior predictive capabilities.

CONCLUSIONS

1. **The numerical simulation of Friction Stir Processing (FSP) provided an accurate prediction of the bead geometry and shape when compared to the experimental results.**
2. **The percentage error between the experimental and Abaqus results is approximately 5.48 %.**
3. **Temperature distribution during processing obtained by SPH method was in good agreement with experimental results obtained by an infrared camera.**
4. **There is good agreement in the results between two methods, CEL (Coupled Eulerian-Lagrangian) and SPH (Smoothed Particle Hydrodynamics).**

5. **At the end of the work piece, the highest temperature reaches 1076 degrees Celsius, but it gradually drops to 400 degrees Celsius at the beginning. The work piece cools down quickly, with a cooling rate of 2.82°C per second. These findings show how temperatures change during the machining process and provide important information for making machining more efficient and improving the quality of the work piece.**

REFERENCES

1. G. Chail and P. Kangas, "Super and hyper duplex stainless steels: structures, properties and applications," Procedia Struct. Integr., vol. 2, pp. 1755–1762, 2016, doi: https://doi.org/10.1016/j.prostr.2016.06.221., (2016)

2. P. Chauhan, R. Jain, S. K. Pal, and S. B. Singh, "Modeling of defects in friction stir welding using coupled Eulerian and Lagrangian method," J. Manuf. Process., vol. 34, pp. 158–166, (2018).

3. A. Tartakovsky, G. Grant, X. Sun, and M. Khaleel, "Modeling of friction stir welding (FSW) process with smooth particle hydrodynamics (SPH)," SAE Technical Paper, (2006).

4. S. M, N. S, and B. S. Davidson, "Friction stir welding parameters and their influence on mechanical properties of welded AA6061 and AA5052 aluminium plates," Mater. Res. Express, vol. 8, no. 10, p. 106525, 2021, doi: 10.1088/2053-1591/ac2daf, (2021).

5. K. Devendranath Ramkumar et al., "Effect of optimal weld parameters in the microstructure and mechanical properties of autogeneous gas tungsten arc weldments of super-duplex stainless steel UNS S32750," Mater. Des., vol. 66, no. PA, pp. 356–365, 2015, doi: 10.1016/j.matdes.2014.10.084, (2014).

6. P. Kah, R. Rajan, J. Martikainen, and R. Suoranta, "Investigation of weld defects in friction-stir welding and fusion welding of aluminium alloys," Int. J. Mech. Mater. Eng., vol. 10, no. 1, 2015, doi: 10.1186/s40712-015-0053-8, (2015).

7. M. Ahmed, S. Ataya, M. El-Sayed Seleman, T. Allam, N. Alsaleh, and E. Ahmed, "Grain Structure, Crystallographic Texture, and Hardening Behavior of Dissimilar Friction Stir Welded AA5083-O and AA5754-H14," Metals (Basel), vol. 11, p. 181, Jan. 2021, doi: 10.3390/met11020181, (2021).

8. W. B. Lee, Y. M. Yeon, and S. B. Jung, "The improvement of mechanical properties of friction-stir-welded A356 Al alloy," Mater. Sci. Eng. A, vol. 355, no. 1–2, pp. 154–159, (2003).

9. B. Darras and E. Kishta, "Submerged friction stir processing of AZ31 Magnesium alloy," Mater. Des., vol. 47, pp. 133–137, (2013).

10. C. Sharma, D. K. Dwivedi, and P. Kumar, "Effect of post weld heat treatments on microstructure and mechanical properties of friction stir welded joints of Al–Zn–Mg alloy AA7039," Mater. Des., vol. 43, pp. 134–143, (2013).

11. F. Al-Badour, N. Merah, A. Shuaib, and A. Bazoune, "Coupled Eulerian Lagrangian finite element modeling of friction stir welding processes," J. Mater. Process. Technol., vol. 213, no. 8, pp. 1433–1439, (2013).

12. M. Akbari and P. Asadi, "Dissimilar friction stir lap welding of aluminum to brass: Modeling of material mixing using coupled Eulerian–Lagrangian method with experimental verifications," Proc. Inst. Mech. Eng. Part L J. Mater. Des. Appl., vol. 234, no. 8, pp. 1117–1128, (2020).

13. K. Fraser, L. I. Kiss, L. St-Georges, and D. Drolet, "Optimization of friction stir weld joint quality using a meshfree fully-coupled thermo-mechanics approach," Metals

(Basel)., vol. 8, no. 2, p. 101, (2018).
14. B. Meyghani, M. B. Awang, and C. S. Wu, "Thermal analysis of friction stir processing (FSP) using arbitrary lagrangian-eulerian (ALE) and smoothed particle hydrodynamics (SPH) meshing techniques," Materwiss. Werksttech., vol. 51, no. 5, pp. 550–557, (2020).
15. Z. Huang, L. Gao, Y. Wang, and F. Wang, "Determination of the Johnson-Cook constitutive model parameters of materials by cluster global optimization algorithm," J. Mater. Eng. Perform., vol. 25, pp. 4099–4107, (2016).
16. R. Franchi, A. Del Prete, and D. Umbrello, "Inverse analysis procedure to determine flow stress and friction data for finite element modeling of machining," Int. J. Mater. Form., vol. 10, pp. 685–695, (2017).
17. M. E. Arafat, F. Al Badour, and N. Merah, "Fully coupled thermo-mechanical finite element modeling of friction stir processing of super duplex stainless steel," Int. J. Adv. Manuf. Technol., vol. 112, pp. 3485–3500, (2021).
18. Eslam A., "Friction stir welding of super duplex stainless steel", A M. Sc. Thesis, Faculty of Engineering, Suez Canal University, EGYPT, (2023).
19. M. Al-Moussawi, A. Smith, A. E. Young, M. Faraji, and S. Cater, "An advanced numerical model of friction stir welding of DH36 steel", (2016).
20. A. Mattsson and M. Lindholm, "Friction and wear mechanisms of PCBN in sliding contact with tool steel", (2011).